

MHD Slip Flow and Heat Transfer of Cu-Fe₃O₄/ Ethylene Glycol-Based Hybrid Nanofluid over a Stretching Surface

Kumaresan Ezhil¹, Sravan Kumar Thavada², Suresh Babu Ramakrishna^{3,*}

¹ Department of Mathematics, Sree Abiraami Arts and Science College for Women, Vellore-632 059, Tamil Nadu, India; kumaresan1504@gmail.com (E.K);

² Department of Mathematics, REVA University, Bangalore-560 064, Karnataka, India; thavadasravankumar@gmail.com (T.S.K.);

³ Department of Mathematics, M. S. Ramaiah Institute of Technology, Bangalore-560 054, Karnataka, India; sureshbabur@msrit.edu (S.B.R.);

* Correspondence: sureshbabur@msrit.edu;

Scopus Author ID:57199323358

Received: 6.11.2020; Revised: 18.12.2020; Accepted: 20.12.2020; Published: 22.12.2020

Abstract: In this article, the impact of hybrid nanoparticles on different physical quantities in a Cu-Fe₃O₄/ethylene glycol-based hybrid nanofluid is associated with a steady and fully developed natural convective flow over a stretching surface. The investigation's significant results are that the ferrous oxide/ethylene glycol-based hybrid nanofluid enlarged with partial slip parameter undermines the tangential velocity and liquid suction. It causes a minute radial velocity along with temperature distribution through a stretching surface. The analysis is presented in dimensionless form. The transformed equations are solved numerically using Fourth order R-K Fehlberg with shooting technique. It is a phenomenon found in a mixture of mobile particles that exhibit specific responses to temperature strength. The particle moves to the hot clod region in thermal diffusion; then it is called 'positive'; otherwise, it is called 'negative'. The consequences of this investigation are of significance with evaluating the impact of some essential design parameters on heat transfer and, therefore, in the enhancement of industrial processes.

Keywords: MHD; hybrid nanofluid; thermal radiation; chemical reaction; porous medium; shooting technique.

List of symbols:

u, v, w	x, y, z velocity components (ms^{-1})	Greek symbols	
Re	Reynolds number	ϕ_1, ϕ_2	Nanoparticles volume fraction
T	The temperature of the fluid (K)	ρ	Fluid density (kg m^{-3})
T_∞	Free stream temperature (K)	μ	Dynamic viscosity ($\text{kg m}^{-1} \text{s}^{-1}$)
T_w	Surface temperature (K)	ν	Kinematic viscosity ($\text{m}^2 \text{s}^{-1}$)
C_p	Specific heat constant pressure ($\text{J kg}^{-1} \text{K}^{-1}$)	σ	Electric conductivity (Sm^{-1})
Pr	Prandtl number	κ	Thermal conductivity ($\text{W m}^{-1} \text{K}^{-1}$)
Ec	Eckert number	ξ	Rate of chemical reaction
B_0	Strength of magnetic field (T)	Ω	Angular velocity
q_r	Radiative heat flux (W.m^{-2})	Sub scripts	
Sc	Schmidt number	f	Base fluid
M	Magnetic number	nf	Nanofluid
C	The concentration of the species	hnf	Hybrid nanofluid

C_w	Uniform constant concentration	bf	Base fluid
C_∞	Free stream concentration	s_1	First solid nanoparticle
K	Permeability parameter	s_2	Second solid nanoparticle
R	Radiation parameter		

© 2020 by the authors. This article is an open-access article distributed under the terms and conditions of the Creative Commons Attribution (CC BY) license (<https://creativecommons.org/licenses/by/4.0/>).

1. Introduction

A wide range of research has recently been carried out on a new generation of nanofluids; such liquids are known as hybrid nanofluids. Hybrid nanofluids have enhanced thermal properties because of a combined impact made by the presence of various substances. This recent development, created by the inclusion of various nanoparticles in the working liquid, has become a common topic among researchers because of its many potential benefits over nanofluids. Many researchers have currently attempted the hybrid nanofluids or mixed, combined or mixed with two different types of nanoparticles. Essentially, the idea of using hybrid nanofluids is to increase thermophysical properties in addition, particularly the charge of the heat switch compared to single-particle nanofluids or standard nanofluids. Since hybrid nanofluids are the latest form of nonliquids, the assessment process for deciding their performance remains within the improvement phase. By using hybrid nanofluids, high performance can be expected in terms of heat transfer. Recently, extended classes of nanofluids have attracted researchers' attention, forming a variety of nanoparticles such as metal particles (Ag, Au, Al, Cu, and Fe), non-metal particles (CuO, TiO₂, Al₂O₃, SiC, and Fe₃O₄); carbon nanotubes. Distinct unitary hybrid nanofluids, nanofluids display uncommon rheological performance and thermo-physicochemical properties. Most significantly, hybrid nanofluids can result in suitable and acceptable nanofluid stability. Those strong nanofluids have proper functions together with better thermal conductivity at lesser nanoparticle concentrations. It also has helpful biomedical production applications, welding, lubrication, power systems, spacecraft, aeronautical device making, and vehicle thermal coordination. The application of nanomaterials for heat transfer enhancement is being widely experimented with by various researchers worldwide. At better heat flux circumstances, conventional liquids cannot achieve the desired heat transfer rate due to their inherently low thermal conductivities. The modern technique for enhancing heat transfer by utilizing ultrafine solid particles in liquids has been widely experimented with over the last decade. Choi [1] proposed the term nanofluid to describe the suspension with high effective thermal conductivity in the base fluid through the diffusion of some nanosized solid particles.

Several experimental types of research have been carried out to investigate the heat transfer properties of hybrid nanoliquids. Suresh *et al.* [2-3] experimentally studied convective heat transfer turbulent flow of Cu-Al₂O₃/H₂O hybrid nanofluids via a circular tube under constant heat flux conditions. They observed that the average increase in Nusselt number for Cu- Al₂O₃/H₂O hybrid nanofluid was 8.02% compared to base fluid (H₂O). The experimental findings show that 0.1% of Cu-Al₂O₃/H₂O hybrid nanofluids have a friction factor significantly slightly higher than 0.1% of Al₂O₃/H₂O nanofluids. Atul Bhattad [4] experimentally investigated the exergy–energy characteristics of Al₂O₃ –MgO hybrid nanofluid, mixed with various base liquids in a plate heat exchanger of the counter flow category in volume with a mixing ratio of 0.01, a volume of flows. The hybrid nanofluid operating temperatures are 30 -

45°C and 2.0 -4.0 L/min, respectively. Their results showed that the performance index of heat exchanger grows by 11.1% for alumina- MgO (4:1) deionized H₂O hybrid nanofluid. Ataei *et al.* [5] investigated the heat transfer and flow properties of a hybrid nanofluid (i.e., TiO₂- Al₂O₃/ H₂O) in a mini channel heat source. They described an increase in the convective heat transfer coefficient compared to pure water by 16.97%. The use of TiO₂- Al₂O₃-H₂O hybrid nanofluid instead of H₂O reduced the wall temperature up to 5 °C. Phanindra *et al.* [6] employed laminar heat transfer of a hybrid nanofluid Al₂O₃-Cu/Oil under a boundary condition of continuous heat flux through a concentric tubular exchanger with a volume concentration of 0.1%. They claimed that the hybrid nanofluid presented the most development of 12.06% in the heat transfer rate at a Reynolds number of 1820 compared to base fluid (pure Oil).

It can be seen that many researchers considered a different type of hybrid nanofluids to enhance thermal conductivity. Taza Gul *et al.* [7] investigated the thin-film flow of the H₂O-based carbon nanotubes hybrid nanofluid. Ogunseye *et al.* [8] examined the viscous dissipation on an Eyring-Powell Cu-Al₂O₃/ethylene glycol nanofluid. Liaquat Ali Lund *et al.* [9] addressed the MHD flow of Cu- Fe₃O₄/ H₂O hybrid nanofluid. Hayat *et al.* [10]) analyzed on the enhancement in heat conduction by employing Ag-CuO/H₂O hybrid nanofluid. Mabood *et al.* [11] examined the Al₂O₃ -Cu-/H₂O hybrid nanofluid flow with melting heat transfer. Aamir Ali *et al.* [12] studied enhancing the thermal conductivity of hybrid nanofluid with Cu-Al₂O₃ nanoparticles. Zhixiong Li *et al.* [13] studied the hydrothermal behavior and the irreversibility of Ag-MgO/H₂O hybrid nanofluid flow numerically through a sinusoidal hairpin heat-exchanger. Benkhedda *et al.* [14] carried out the combined convective heat transfer improvement using TiO₂-Ag/ H₂O hybrid nanofluid in a heated horizontal ring. Hassan *et al.* [15] studied the homotopic analysis to elucidate the effects of an inclined magnetic field and nonlinear thermal radiation on the melting energy transmission in stagnation point flow over a stretchable sheet. Rahman *et al.* [16] carried out the transient MHD flow of water-based nanofluids along a straight-up solid porous wall against the horizon with the time-dependent plate velocity, temperature, and concentration. They computed the results by fixing the Prandtl number at $Pr=0.71$ (air), which is not valid for water-based nanofluids. Their results are unrealistic. Takabi and Shokouhmand [17] studied the rate of molecular species diffusion effects on MHD gravity-driven convective flow of nanofluids over an oscillating vertical plate Laplace transform method. The results were presented for inappropriate magnitudes of Schmidt number.

The involvement of magnetohydrodynamic in boundary layer flow controls the flow of the fluid by connecting fluid flow with magnetic fields. There has been much research on magnetohydrodynamic flow in the past. Magnetohydrodynamic flow is described as studying the magnetic properties and behavior of electro-conductive fluids through a magnetic field [18-29].

Based on the literature review, the present paper is to provide an impact of viscous dissipation and thermal radiation on MHD hybrid nanofluid flow with the combined effects of melting heat transfer and partial slip has not been previously studied. The analysis is presented in dimensionless form. The transformed equations are solved numerically using Fourth order R-K Fehlberg with shooting technique. Using these computations of the tangential velocity, temperature, and concentration have been plotted graphically to analyze the effects of various physical parameters in the problem. Also, the physical interpretation examined the skin-friction coefficient. The rate at which heat affects the boundary layer's vicinity is also presented and

discussed in detail. New insights from this study will be useful in several areas of nanotechnology and nanostructure.

2. Materials and Methods

2.1. Mathematical formulation.




The problem's physical model is considered the 3D steady MHD hybrid nanofluid flow over a stretching sheet. The fluid occupies $z > 0$, and the flow is induced due to the stretching of the sheet $z = 0$ along the x – and y –axis with the velocities $U_w = ax$ $V_w = by$ and, where $a > 0, b > 0$ are the stretching rates of the sheet (see Fig.1). The surface temperature and concentration are subjected to partial slip, and so is $T_w + l \frac{\partial T}{\partial z}$, $C_w + l \frac{\partial C}{\partial z}$ where l is the thermal slip factor. The nanofluid is turning about the vertical z – axis with the angular velocity Ω of the fluid is stable.

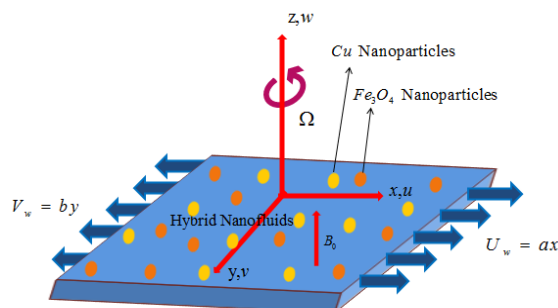
Table 1. Thermophysical properties of $C_2H_6O_2$ and nanoparticles at $T=300K$ [26, 27, 28, 29].

Physical properties	Pure water	Ethylene glycol ($C_2H_6O_2$)	Cu(copper)	Fe_3O_4 (Iron oxide)
$\rho (kg / m^3)$	997.1	1115	8933	5180
$c_p (J / kg.K)$	4179	2430	385	670
$\kappa (W / m.K)$	0.613	0.253	401	9.7
Pr	6.8377	24.4	-	-

A static magnetic field B_0 is imposed normal (perpendicular) to the stretching surface. It also assumed that the magnetic Reynolds number is not significant in the free convection flow; consequently, the induced magnetic field is ignored. The surface temperature is adjusted by the convection process through the hotted fluid with temperature T_f T_∞ and represents the ambient temperature. Ethylene glycol is the base fluid. The silver and copper are used as nanoparticles.

Table 2. Shape factor values various nanoparticle shapes [27, 28].

Particle shapes	Spherical	Cylinder	Platelet
			
n	3	4.8	5.7



$$u = U_w + kv_f \frac{\partial u}{\partial z}, v = V_w + kv_f \frac{\partial v}{\partial z}, w = 0, T = T_w + l \frac{\partial T}{\partial z}, C = C_w + l \frac{\partial C}{\partial z}$$

Figure 1. Geometry of the problem.

The equations of the flow problem are defined as:

$$\frac{\partial u}{\partial x} + \frac{\partial v}{\partial y} + \frac{\partial w}{\partial z} = 0, \quad (1)$$

$$u \frac{\partial u}{\partial x} + v \frac{\partial u}{\partial y} + w \frac{\partial u}{\partial z} - 2\Omega v = \frac{1}{\rho_{hmf}} \left[\mu_{hmf} \frac{\partial^2 u}{\partial z^2} - \sigma B_0^2 u - \frac{\mu_{hmf}}{k} u \right], \quad (2)$$

$$u \frac{\partial v}{\partial x} + v \frac{\partial v}{\partial y} + w \frac{\partial v}{\partial z} + 2\Omega u = \frac{1}{\rho_{hmf}} \left[\mu_{hmf} \frac{\partial^2 v}{\partial z^2} - \sigma B_0^2 v - \frac{\mu_{hmf}}{k} v \right], \quad (3)$$

$$u \frac{\partial T}{\partial x} + v \frac{\partial T}{\partial y} + w \frac{\partial T}{\partial z} = \alpha_{hmf} \frac{\partial^2 T}{\partial z^2} - \frac{1}{(\rho C_p)_{hmf}} \frac{\partial q_r}{\partial z} + \frac{\mu_{hmf}}{(\rho C_p)_{hmf}} \left[\left(\frac{\partial u}{\partial z} \right)^2 + \left(\frac{\partial v}{\partial z} \right)^2 \right], \quad (4)$$

$$u \frac{\partial C}{\partial x} + v \frac{\partial C}{\partial y} + w \frac{\partial C}{\partial z} = \beta_{hmf} \frac{\partial^2 C}{\partial z^2} - \xi (C - C_\infty)^n. \quad (5)$$

The endpoint conditions are

$$u = U_w + kv_f \frac{\partial u}{\partial z}, \quad v = V_w + kv_f \frac{\partial v}{\partial z}, \quad w = 0, \quad T = T_w + l \frac{\partial T}{\partial z}, \quad C = C_w + l \frac{\partial C}{\partial z} \quad \text{at} \quad z = 0, \\ u \rightarrow 0, \quad v \rightarrow 0, \quad T \rightarrow T_\infty, \quad C \rightarrow C_\infty \quad \text{as} \quad z \rightarrow \infty. \quad (6)$$

Radiative heat flux is approximated using Rosseland approximation in the following from

$$q_r = -\frac{4\sigma}{3\chi} \frac{\partial T^4}{\partial z} \quad (7)$$

Where, σ and χ are the “Stephan-Boltzman constant” and the mean absorption coefficient

$$T^4 = T_\infty^4 + 4T_\infty^3 (T - T_\infty) + 6T_\infty^2 (T - T_\infty)^2 + \dots \quad (8)$$

Neglecting higher-order terms in the above equation (8) beyond the first degree in $(T - T_\infty)$, we get

$$T^4 \cong 4TT_\infty^3 - 3T_\infty^4 \quad (9)$$

Thus, substituting Eq. (9) into Eq. (7) we get

$$\frac{\partial q_r}{\partial z} = -\frac{16\sigma T_\infty^3}{3\chi} \frac{\partial^2 T}{\partial z^2}. \quad (10)$$

Therefore equation (4) reduced to

$$u \frac{\partial T}{\partial x} + v \frac{\partial T}{\partial y} + w \frac{\partial T}{\partial z} = \alpha_{hmf} \frac{\partial^2 T}{\partial z^2} + \frac{1}{(\rho C_p)_{hmf}} \frac{16\sigma T_\infty^3}{3\chi} \frac{\partial^2 T}{\partial z^2} + \frac{\mu_{hmf}}{(\rho C_p)_{hmf}} \left[\left(\frac{\partial u}{\partial z} \right)^2 + \left(\frac{\partial v}{\partial z} \right)^2 \right] \quad (11)$$

By introducing the following dimensionless quantities:

$$v = ayq'(\eta), \quad u = axp'(\eta), \quad w = -\sqrt{av_f} (p(\eta) + q(\eta)), \quad \eta = z \sqrt{\frac{a}{v_f}}, \quad \theta(\eta) = \frac{T - T_\infty}{T_w - T_\infty}, \quad (12)$$

$$R(\eta) = \frac{C - C_\infty}{C_w - C_\infty}.$$

2.1.1. Thermophysical properties of nanofluid and hybrid nanofluid.

Thermophysical properties are defined as follows:

The density, heat capacitance, effective thermal conductivity, and viscosity of the nanofluid are given by:

$$\rho_{nf} = (1 - \phi) \rho_f + \phi \rho_s;$$

$$\begin{aligned}(\rho C_p)_{nf} &= (1-\phi)(\rho C_p)_f + \phi(\rho C_p)_s \\ \frac{\kappa_{nf}}{\kappa_f} &= \frac{\kappa_s + (n-1)\kappa_f - (n-1)\phi(\kappa_f - \kappa_s)}{\kappa_s + (n-1)\kappa_f + \phi(\kappa_f - \kappa_s)}, \text{ where } n = 3/\psi \\ \mu_{nf} &= \frac{\mu_f}{(1-\phi)^{2.5}}\end{aligned}$$

Thermophysical properties of Cu-Fe₃O₄-Ethylene glycol nanofluid are defined as follows:
The density, heat capacitance, effective thermal conductivity, and viscosity gave by:

$$\begin{aligned}\rho_{hnf} &= \left[(1-\phi_2) \left\{ (1-\phi_1)\rho_f + \phi_1\rho_{s1} \right\} \right] + \phi_2\rho_{s2}; \\ (\rho C_p)_{hnf} &= \left[(1-\phi_2) \left\{ (1-\phi_1)(\rho C_p)_f + \phi_1(\rho C_p)_{s1} \right\} \right] + \phi_2(\rho C_p)_{s2} \\ \frac{\kappa_{bf}}{\kappa_f} &= \frac{\kappa_{s1} + (n-1)\kappa_f - (n-1)\phi_1(\kappa_f - \kappa_{s1})}{\kappa_{s1} + (n-1)\kappa_f + \phi_1(\kappa_f - \kappa_{s1})}; \quad \frac{\kappa_{hnf}}{\kappa_f} = \frac{\kappa_{s2} + (n-1)\kappa_{bf} - (n-1)\phi_2(\kappa_{bf} - \kappa_{s2})}{\kappa_{s2} + (n-1)\kappa_{bf} + \phi_2(\kappa_{bf} - \kappa_{s2})} \\ \mu_{hnf} &= \frac{\mu_f}{(1-\phi_1)^{2.5}(1-\phi_2)^{2.5}}\end{aligned}$$

The above governing equations are reduced to

$$p'''(\eta) - (1-\phi_1)^{2.5}(1-\phi_2)^{2.5} \left[(1-\phi_2) \left\{ (1-\phi_1) + \phi_1 \left(\frac{\rho_{s1}}{\rho_f} \right) \right\} + \phi_2 \left(\frac{\rho_{s2}}{\rho_f} \right) \right] \quad (13)$$

$$\times \left[(p'(\eta))^2 - p''(\eta)(p(\eta) + q(\eta)) - 2\gamma\delta q'(\eta) \right] - (1-\phi_1)^{2.5}(1-\phi_2)^{2.5} M^2 p'(\eta) - Kp'(\eta) = 0$$

$$q'''(\eta) - (1-\phi_1)^{2.5}(1-\phi_2)^{2.5} \left[(1-\phi_2) \left\{ (1-\phi_1) + \phi_1 \left(\frac{\rho_{s1}}{\rho_f} \right) \right\} + \phi_2 \left(\frac{\rho_{s2}}{\rho_f} \right) \right] \quad (14)$$

$$\times \left[(q'(\eta))^2 - q''(\eta)(p(\eta) + q(\eta)) - \frac{2\gamma}{\delta} p'(\eta) \right] - (1-\phi_1)^{2.5}(1-\phi_2)^{2.5} M^2 q'(\eta) - Kq'(\eta) = 0$$

$$\left(\frac{\kappa_{hnf}}{\kappa_f} + \frac{4}{3}R \right) \theta''(\eta) + \left[(1-\phi_2) \left\{ (1-\phi_1) + \phi_1 \left(\frac{(\rho C_p)_{s1}}{(\rho C_p)_f} \right) \right\} + \phi_2 \left(\frac{(\rho C_p)_{s2}}{(\rho C_p)_f} \right) \right] \quad (15)$$

$$\times \text{Pr} (p(\eta) + q(\eta)) \theta'(\eta) + \text{Pr} Ec \left((p''(\eta))^2 + \delta^2 (q''(\eta))^2 \right) = 0$$

$$R''(\eta) + \frac{Sc}{(1-\phi_1)(1-\phi_2)} \left[(p(\eta) + q(\eta)) R'(\eta) - R_c R(\eta) \right] = 0 \quad (16)$$

The corresponding transformed boundary conditions are

$$\begin{aligned}p &= 0, \quad p'(\eta) = 1 + \alpha p''(0), \quad q = 0, \quad q'(\eta) = \lambda + \alpha q''(0), \\ \theta(\eta) &= 1 + \beta_1 \theta'(0), \quad R(\eta) = 1 + \beta_2 R'(0) \quad \text{at } \eta = 0 \\ p' &\rightarrow 0, \quad q' \rightarrow 0, \quad \theta \rightarrow 0, \quad R \rightarrow 0 \quad \text{as } \eta \rightarrow \infty\end{aligned} \quad (17)$$

Non-dimensional quantities are

$$\gamma = \frac{\Omega}{a}, \alpha = k\sqrt{av_f}, \beta = l\sqrt{\frac{a}{v_f}}, \lambda = \frac{b}{a}, R = \frac{4\sigma T_\infty^3}{\chi\kappa_f}, \delta = \frac{y}{x} = \frac{\sqrt{\frac{a}{v_f}}y}{\sqrt{\frac{a}{v_f}}x}, M = \sqrt{\frac{\sigma B_0^2}{a\rho_f}} \quad (18)$$

$$Pr = \frac{(\mu C_p)_f}{\kappa_f}, Ec = \frac{U_w^2}{(C_p)_f (T_w - T_\infty)}, K_1 = \frac{\mu_f}{ak\rho_f}, Sc = \frac{\nu_f}{\beta_f}, R_c = \frac{\xi(C - C_\infty)^{n-1}}{a}$$

For mathematical and engineering point of concern, the skin friction coefficient, the reduced Nusselt number, and the Sherwood number are as follows

$$C_{fx} = \frac{\mu_{hmf}}{\rho_f(ax)^2} \left(\frac{\partial u}{\partial z} \right) \bigg|_{z=0}, \quad C_{fy} = \frac{\mu_{hmf}}{\rho_f(ax)^2} \left(\frac{\partial v}{\partial z} \right) \bigg|_{z=0}, \quad N_{ux} = -\frac{x\kappa_{hmf}}{\kappa_f(T_w - T_\infty)} \left(\frac{\partial T}{\partial z} \right) \bigg|_{z=0}$$

$$S_{hx} = -\frac{x}{(C_w - C_\infty)} \left(\frac{\partial C}{\partial z} \right) \bigg|_{z=0};$$

$$Re^{\frac{1}{2}} C_{fx} = \frac{1}{(1-\phi_1)^{2.5} (1-\phi_2)^{2.5}} p''(0), \quad \delta^{-1} Re^{\frac{1}{2}} C_{fy} = \frac{1}{(1-\phi_1)^{2.5} (1-\phi_2)^{2.5}} q''(0),$$

$$Re^{-\frac{1}{2}} N_{ux} = -\left(\frac{\kappa_{hmf}}{\kappa_f} + \frac{4}{3} R \right) \theta'(0), \quad Re^{-\frac{1}{2}} S_{hx} = -R'(0);$$

Where $Re = \frac{U_w x}{\nu_f}$ is the local Reynolds number.

3. Results and Discussion

The system of moderated coupled nonlinear ODE's (13)-(16) including a new set of subject to condition (17) is utilized R-K-Fehlberg-integration with shooting method. The impacts of different governing dimensionless parameters are inspected, the Magnetic parameter M , Porous medium parameter K_1 , Rotation parameter γ , Eckert number Ec , Chemical reaction parameter Rc , Schmidt number Sc , Prandtl number Pr , Thermal jump parameter β , velocity slip parameter α , Thermal radiation parameter R on the velocities $p'(\eta)$, $q'(\eta)$, temperature $\theta(\eta)$, and concentration $R(\eta)$ fields, which are portrayed via Figs.2-17.

The performance of magnetic parameter M on stream components $p'(\eta)$ and temperature dispersal $\theta(\eta)$ is explained in Figs.2-3. With the influence of M in an electrically conducting liquid, drug-like energy is established. This resistive energy tends to slow the fluid movement at the expense of temperature improvement over the surface. This is often depicted by the decrease within the velocity values, which is found in Fig. 2. Because of a decrease in velocities components, an improvement happens in liquid temperature, as saw in Fig. 3.

The assessment between a base liquid (Ethylene glycol), a Cu- Ethylene glycol, and Cu- Fe₃O₄/ Ethylene glycol on transverse velocity and the degrees of hotness distributions is introduced in Figs. 4-5 Here, we see that compared to nanofluid (Cu-C₂H₆O₂) and hybrid nanofluid (Cu- Fe₃O₄/ C₂H₆O₂) of base fluid (C₂H₆O₂). The velocity is high, but the opposite is true concerning temperature. It is found that the transverse velocity of the base liquid (Ethylene glycol) is more prominent as compared to the Cu-Ethylene glycol and Cu- Fe₃O₄/

C₂H₆O₂. However, the reverse trend is viewed in the temperature profile. The temperature for the Cu- Fe₃O₄/ C₂H₆O₂ is greater than the C₂H₆O₂ and Cu-C₂H₆O₂. Physically, nanoparticles dissipate heat in the form of heat. Consideration of more nanoparticles can lead to more radiation that escalates the temperature.

Figs. 6-7 are drawn to investigate the effects of the velocity slip parameter α on the transverse velocity distributions of $p'(\eta)$, and $q'(\eta)$. It can be observed from these that the transverse velocity slip parameter α brings about a remarkable drop in the transverse velocity distribution $p'(\eta)$ and $q'(\eta)$ for both liquids. This is because, within sight of slip, the fluid's velocity near the surface doesn't continue as correspondingly for the stretching surface velocity. Therefore, the slip velocity intensifies by escalates the velocity slip parameter α . This is followed by reducing the liquid velocity because the deformation of the stretching surface, under the slip conditions, can only be transferred to the fluid.

The impact of the γ over the transverse velocity and temperature profiles are presented in Fig. 8. From this figure, we can see that increasing the rotation parameters γ significantly reduces the nanofluid's velocities (Cu- C₂H₆O₂) and the hybrid nanofluid (Cu- Fe₃O₄/ C₂H₆O₂). Fig. 9. Shows the impact of permeable media on $p'(\eta)$. It is seen that the velocities of both nanofluids and hybrid nanofluids decrease as the parameter of the permeable media growth.

Fig. 10. It shows that the velocity escalates with the growth δ . The Eckert number refers to the association between enthalpy and kinetic energy. It converts the conservation of kinetic energy into internal energy by work done against the viscous fluid stress. With the aid of action against viscous fluid tension, it transforms the conservation of kinetic energy into internal energy. The positive Ec represents the diminishing concerning heat beside the sheet to the fluid. Fig. 11 shows that heat is transferred from the sheet to the nanofluid, in this manner increasing the temperature of the nanofluid. Fig. 12 shows the importance of the thermal slip parameter β on the temperature field. The temperature profile is reduced by escalates the thermal slip parameter. Physically, less heat is transferred from the surface to the liquid as the thermal slip parameter grows, decreasing the temperature.

Fig. 13 represents the impact of thermal distribution $\theta(\eta)$ for different values of R . It is clear that the distribution of temperature at the boundary layer improves with varying values of the thermal radiation parameter. The effect of thermal radiation is to improve heat transfer because the thermal boundary layer increases with increasing thermal radiation. Therefore, it has been reported that the process of reducing thermal radiation should proceed at a faster rate. Fig. 14. This shows that the concentration field changes in Schmidt number hydrogen gasses, water vapor, and ammonia. It is found that the concentration field of carbon dioxide for hydrogen escalates regularly compared to water vapor. In this manner, water vapor can be utilized to maintain a concentration field, and hydrogen can be used to maintain a well-concentrated field. As the Schmidt number increasing, the concentration reduces with the thickness of the boundary layer. The concentration profiles for R_c is shown in Fig. 15. It is seen that enhancing the values of chemical reaction reduced the liquid. As a result, the thickness of the concentration boundary layer escalates.

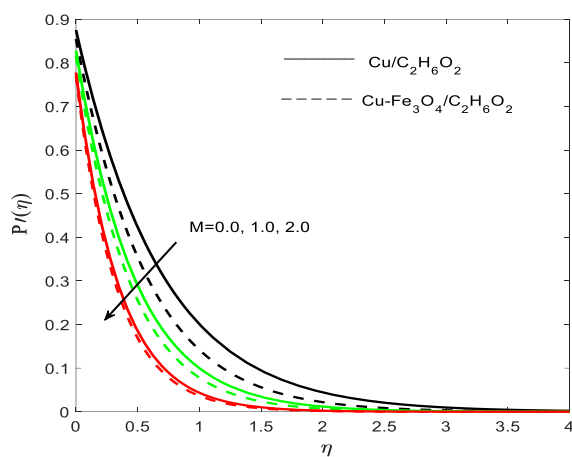


Figure 2. Influence of $P'(\eta)$ for M .

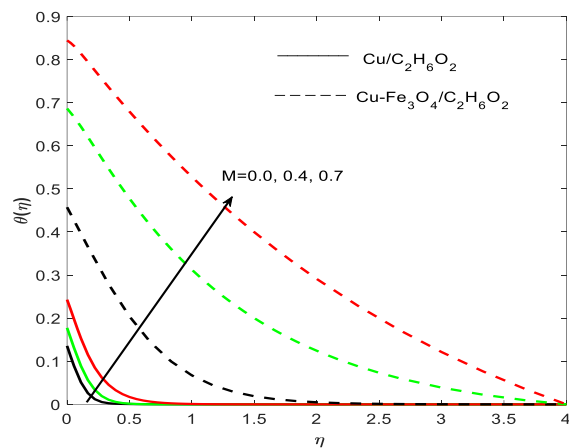


Figure 3. Influence of $\theta(\eta)$ for M .

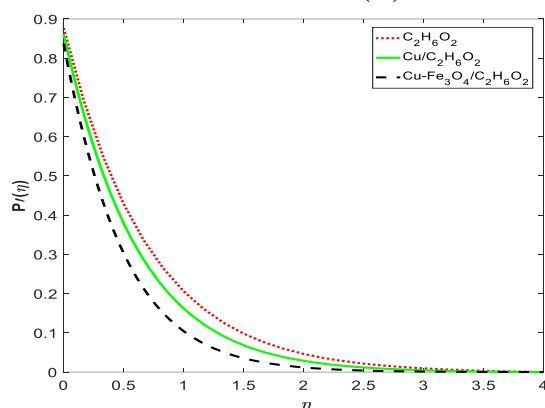


Figure 4. Influence of $P'(\eta)$ for nanofluid.

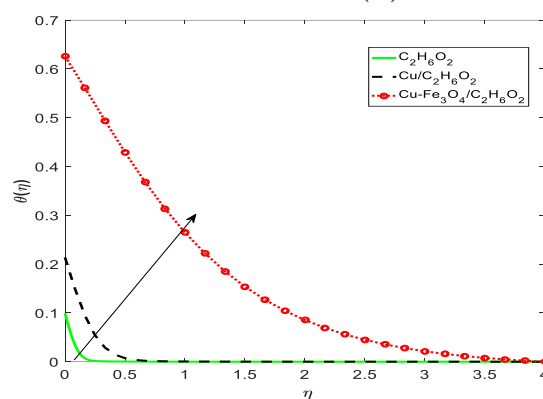


Figure 5. Influence of $\theta(\eta)$ for nanofluid.

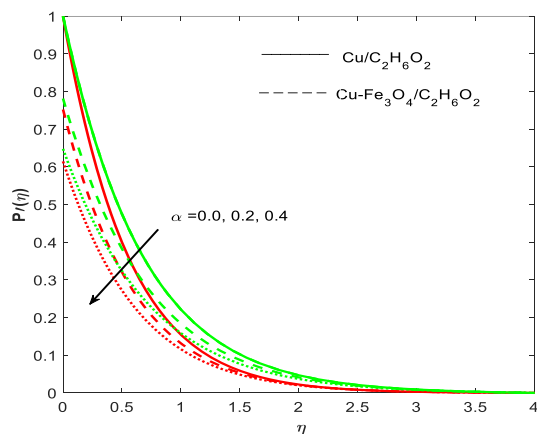


Figure 6. Influence of $P'(\eta)$ for α .

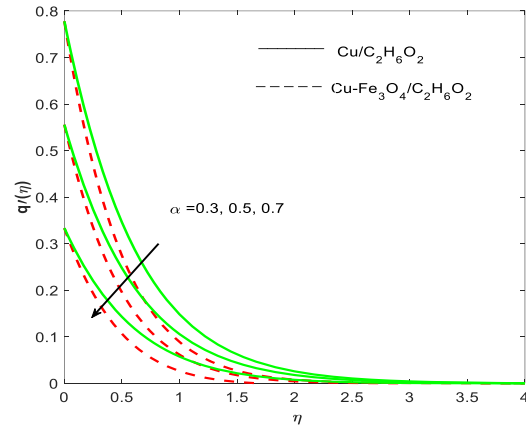


Figure 7. Influence of $\theta(\eta)$ for α .

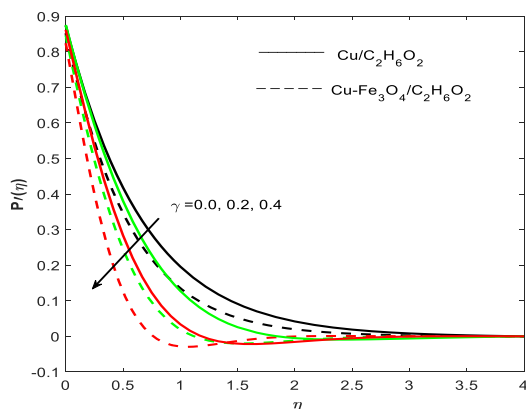


Figure 8. Influence of $P'(\eta)$ for γ .

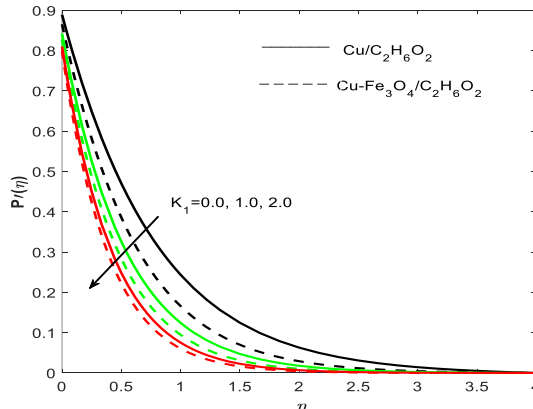


Figure 9. Influence of $P'(\eta)$ for K_1 .

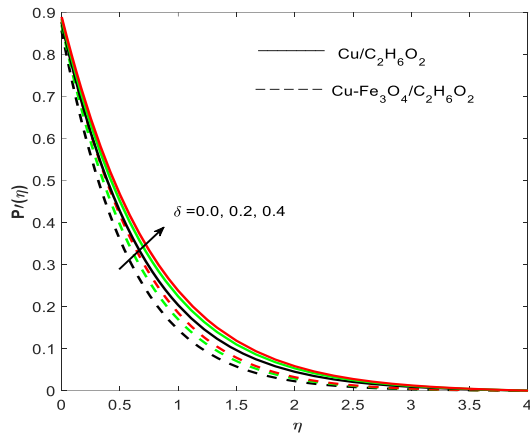


Figure 10. Influence of $P'(\eta)$ for δ .

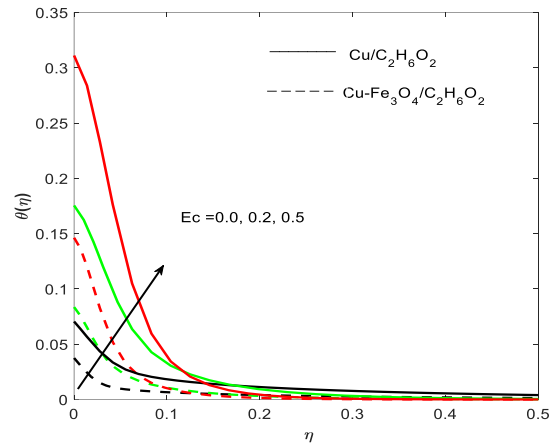


Figure 11. Influence of $\theta(\eta)$ for Ec .

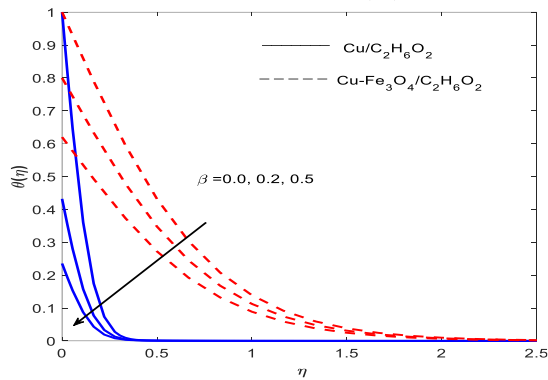


Figure 12. Influence of $\theta(\eta)$ for β .

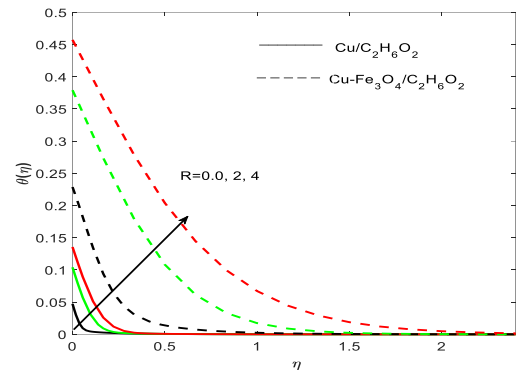


Figure 13. Influence of $\theta(\eta)$ for R .

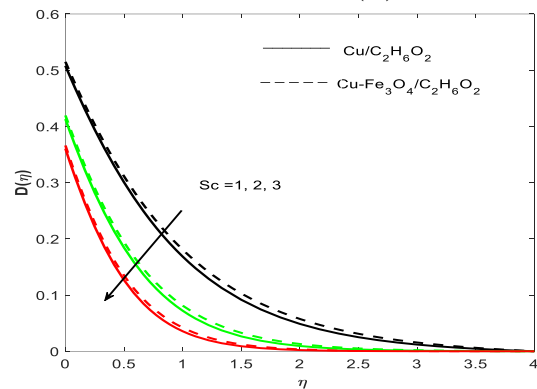


Figure 14. Influence of $R(\eta)$ for Sc .

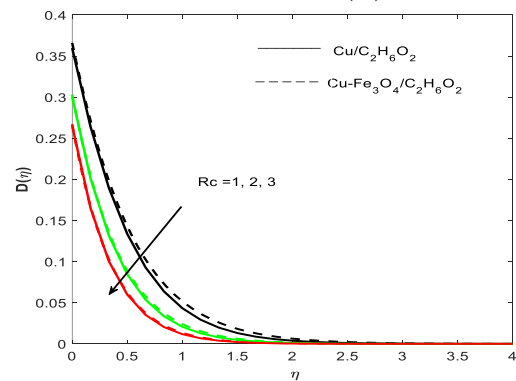


Figure 15. Influence of $R(\eta)$ for Rc .

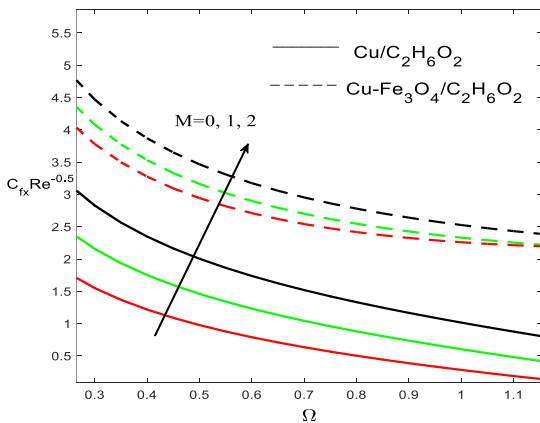


Figure 16. $C_{fx} \text{Re}^{\frac{1}{2}}$ for M for nanofluid and hybrid nanofluid in y direction.

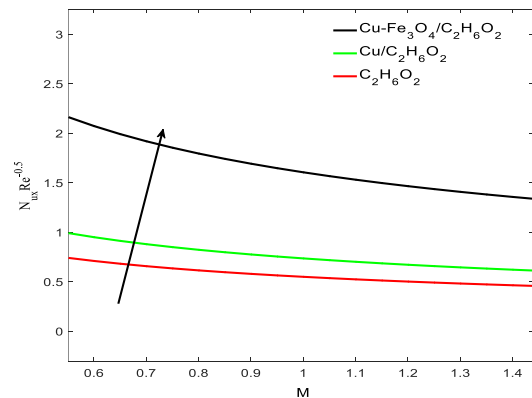


Figure 17. $N_{ux} \text{Re}^{\frac{1}{2}}$ for nanofluid and hybrid nanofluid in y direction

Fig. 16 elucidates the influence of M and $\Omega C_{fx} \text{Re}^{\frac{1}{2}}$ on. It is noticed that skin friction enhances for higher values of M while it increases via Ω . Impact of the base fluid, nanofluid, and hybrid nanofluid on heat transfer presented in Fig. 17 the rate of heat transfer is less for base fluid as compared to the $Cu / C_2H_6O_2$, and $Cu - Fe_3O_4 / C_2H_6O_2$. Thus, the rate at which heat is higher transit is higher for hybrid nanofluids than the Ethylene glycol. Table 3 shows the numerical values of the friction factor for $M \Omega, \gamma, \phi_2$.

Table 3. $C_{fx} \text{Re}^{\frac{1}{2}}, P''(0), q''(0)$ for $Cu / C_2H_6O_2$ and $Cu - Fe_3O_4 / C_2H_6O_2$ with $\phi_1 = 0.1$.

M	Ω	γ	ϕ_2	$\frac{-P''(0)}{(1-\phi_1)^{2.5}}$	$\frac{-P''(0)}{(1-\phi_1)^{2.5}(1-\phi_2)^{2.5}}$	$\frac{-q''(0)}{(1-\phi_1)^{2.5}}$	$\frac{-q''(0)}{(1-\phi_1)^{2.5}(1-\phi_2)^{2.5}}$
0.0	0.1	0.5	0.05	2.14464	2.28453	1.28679	1.48516
0.5				1.84580	2.14121	1.54525	1.58270
1.0				1.94641	2.36551	1.63747	1.68994
1.5				2.41543	2.83606	1.96505	2.27353
	0.2			1.85341	2.30152	1.43147	1.89894
	0.3			1.88474	2.31105	1.96515	2.28078
	0.5			1.99092	2.42500	0.92152	1.16418
		0.2		1.89593	2.43401	0.81552	1.15529
		0.4		1.94542	2.32153	1.43346	1.67775
		0.6		1.77374	2.20006	2.67838	2.01750
			0.04	1.91633	2.21470	1.51564	1.76095
			0.08	2.15620	2.64647	1.75420	2.13190
			0.1	2.28421	2.92372	1.97656	2.50133

We observed that, the skin friction coefficient enhances for intensified values of the magnetic parameter, Angular velocity, rotation parameter ϕ_2 .

4. Conclusions

The convective heat transfer and hybrid nanofluid flow over a sheet with slip impacts. Hybrid nanofluid is considered by suspending two different nanoparticles, which are Cu and then Fe_3O_4 is $C_2H_6O_2$. When utilizing the similarity transformations, the overseeing conditions with boundary conditions must be transformed into a system of ODEs, discussed graphically. The main conclusions are summarized as follows: It is noticed that the hybrid nanofluid $Cu - Fe_3O_4 / C_2H_6O_2$ is best as a heater on growing M . Conversely, on increasing Ec , the slip parameters and stretching, it is higher as a cooler (warmer) in contrasting $Fe_3O_4 / C_2H_6O_2$ ($Cu / C_2H_6O_2$); The hotness of the nanofluid grows with increasing of Eckert number; A decrease in the fluid velocity is observed for higher values of the velocity slip parameter; The transverse velocity profile reduces with increasing solid volume fraction and porous medium but a reverse trend is observed with the increments of γ, K_1, α parameters; The nanofluid velocity decreases as the existence of the M becomes stronger; The rate at which heat transfer occurs for $Cu / C_2H_6O_2$ is the highest among $Cu - Fe_3O_4 / C_2H_6O_2$ nanofluids.

Funding

This research received no external funding.

Acknowledgments

The authors would like to thank the anonymous reviewers for their valuable comments and suggestions to improve the paper's quality.

Conflicts of Interest

The authors declare no conflict of interest.

References

1. Ali, A.; Noreen, A.; Saleem, S.; Aljohani, A.F.; Awais, M. Heat transfer analysis of Cu–Al₂O₃ hybrid nanofluid with heat flux and viscous dissipation. *Journal of Thermal Analysis and Calorimetry* **2020**, 1-11, <https://doi.org/10.1007/s10973-020-09910-6>.
2. Takabi, B.; Shokouhmand, H. Effects of Al₂O₃-Cu/water hybrid nanofluid on heat transfer and flow characteristics in turbulent regime. *International Journal of Modern Physics C* **2015**, *26*, <https://doi.org/10.1142/S0129183115500473>.
3. Bhattad, A. Experimental investigation of Al₂O₃–MgO hot hybrid nanofluid in a plate heat exchanger. *Heat Transfer* **2020**, *49*, 2344-2354, <https://doi.org/10.1002/hjt.21724>.
4. Choi, S.U.S. Enhancing Thermal Conductivity of Fluids with Nanoparticles. *Proceedings of the ASME International Mechanical Engineering Congress and Exposition* **1995**, *66*, 99-105.
5. Cimpean, D.S.; Sheremet, M.A.; Pop, I. Mixed convection of hybrid nanofluid in a porous trapezoidal chamber. *International Communications in Heat and Mass Transfer* **2020**, *116*, <https://doi.org/10.1142/s0129183115500473>.
6. Aly, E.H.; Pop, I. MHD flow and heat transfer near stagnation point over a stretching/shrinking surface with partial slip and viscous dissipation: Hybrid nanofluid versus nanofluid. *Powder Technology* **2020**, *367*, 192-205, <https://doi.org/10.1016/j.powtec.2020.03.030>.
7. Ogunseye, H.A.; Tijani, Y.O.; Sibanda, P. Entropy generation in an unsteady Eyring-Powell hybrid nanofluid flow over a permeable surface: A Lie group analysis. *Heat Transfer* **2020**, *49*, 3374-3390, <https://doi.org/10.1002/hjt.21778>.
8. Hayat, T.; Nadeem, S.; Khan, A.U. Rotating flow of Ag-CuO/H₂O hybrid nanofluid with radiation and partial slip boundary effects. *The European Physical Journal E* **2018**, *41*, 1-9, <https://doi.org/10.1140/epje/i2018-11682-y>.
9. Hayat, T.; Nadeem, S.; Khan, A.U. Numerical analysis of Ag–CuO/water rotating hybrid nanofluid with heat generation and absorption. *Canadian Journal of Physics* **2018**, *97*, 644-650, <https://doi.org/10.1139/cjp-2018-0011>.
10. Tilili, I.; Nabwey, H.A.; Samrat, S.P.; Sandeep, N. 3D MHD nonlinear radiative flow of CuO–MgO/methanol hybrid nanofluid beyond an irregular dimension surface with slip effect. *Scientific Reports* **2020**, *10*, 1-4, <https://doi.org/10.1038/s41598-020-66102-w>.
11. Kumaresan, E.; Vijaya Kumar, A.G. Chemically reactive 3D nonlinear magneto hydrodynamic rotating flow of nanofluids over a deformable surface with joule heating through porous medium. *Trends in Maths* **2019**, 313-323.
12. Lund, L.A.; Omar, Z.; Raza, J.; Khan, I. Magnetohydrodynamic flow of Cu–Fe₃O₄/H₂O hybrid nanofluid with effect of viscous dissipation: dual similarity solutions. *Journal of Thermal Analysis and Calorimetry* **2020**, 1-13, <https://doi.org/10.1007/s10973-020-09602-1>.
13. Mabood, F.; Yusuf, T.A.; Khan, W.A. Cu–Al₂O₃–H₂O hybrid nanofluid flow with melting heat transfer, irreversibility analysis and nonlinear thermal radiation. *Journal of Thermal Analysis and Calorimetry* **2020**, 1-12, <https://doi.org/10.1007/s10973-020-09720-w>.
14. Benkhedda, M.; Boufendi, T.; Touahri, S. Laminar mixed convective heat transfer enhancement by using Ag-TiO₂-water hybrid Nanofluid in a heated horizontal annulus. *Heat and Mass Transfer* **2018**, *54*, 2799-2814, <https://doi.org/10.1007/s00231-018-2302-x>.
15. Ataei, M.; Sadegh Moghanlou, F.; Noorzadeh, S.; Vajdi, M.; Shahedi Asl, M. Heat transfer and flow characteristics of hybrid Al₂O₃/TiO₂–water nanofluid in a minichannel heat sink. *Heat and Mass Transfer* **2020**, *56*, 2757-2767, <https://doi.org/10.1007/s00231-020-02896-9>.
16. Rahman, M.R.A.; Leong, K.Y.; Idris, A.C.; Saad, M.R.; Anwar, M. Numerical analysis of the forced convective heat transfer on Al₂O₃–Cu/water hybrid nanofluid. *Heat and Mass Transfer* **2017**, *53*, 1835-1842, <https://doi.org/10.1007/s00231-016-1941-z>.
17. Hassan, M.; Marin, M.; Ellahi, R.; Alamri, S.Z. Exploration of convective heat transfer and flow characteristics synthesis by Cu–Ag/water hybrid-nanofluids. *Heat Transfer* **2018**, *49*, 1837-1848, <https://doi.org/10.1615/heattransres.2018025569>.

18. Nawaz, M.; Nazir, U.; Saleem, S.; Alharbi, S.O. An enhancement of thermal performance of ethylene glycol by nano and hybrid nanoparticles. *Physica A: Statistical Mechanics and its Applications* **2020**, *551*, <https://doi.org/10.1016/j.physa.2020.124527>.
19. Aladdin, N.A.L.; Bachok, N.; Pop, I. Cu-Al₂O₃/water hybrid nanofluid flow over a permeable moving surface in presence of hydromagnetic and suction effects. *Alexandria Engineering Journal* **2020**, *59*, 657-666, <https://doi.org/10.1016/j.aej.2020.01.028>.
20. Phanindra, Y.; Kumar, S.D.; Pugazhendhi, S. Experimental Investigation on Al₂O₃ & Cu/Oil Hybrid Nano fluid using Concentric Tube Heat Exchanger. *Materials Today: Proceedings* **2018**, *5*, 12142-12150, <https://doi.org/10.1016/j.matpr.2018.02.192>.
21. Shah, Z.; Alzahrani, E.O.; Dawar, A.; Ullah, A.; Khan, I. Influence of Cattaneo-Christov model on Darcy-Forchheimer flow of Micropolar Ferrofluid over a stretching/shrinking sheet. *International Communications in Heat and Mass Transfer* **2020**, *110*, <https://doi.org/10.1016/j.icheatmasstransfer.2019.104385>.
22. Sheikholeslami, M.; Hatami, M.; Ganji, D.D. Micropolar fluid flow and heat transfer in a permeable channel using analytical method. *Journal of Molecular Liquids* **2014**, *194*, 30-36, <https://doi.org/10.1016/j.molliq.2014.01.005>.
23. Subhani, M.; Nadeem, S. Numerical analysis of 3D micropolar nanofluid flow induced by an exponentially stretching surface embedded in a porous medium. *The European Physical Journal Plus* **2017**, *132*, 1-12, <https://doi.org/10.1140/epjp/i2017-11660-0>.
24. Suresh, S.; Venkitaraj, K.P.; Selvakumar, P.; Chandrasekar, M. Effect of Al₂O₃-Cu/water hybrid nanofluid in heat transfer. *Experimental Thermal and Fluid Science* **2012**, *38*, 54-60, <https://doi.org/10.1016/j.expthermflusci.2011.11.007>.
25. Suresh, S.; Venkitaraj, K.P.; Hameed, M.S.; Sarangan, J. Turbulent Heat Transfer and Pressure Drop Characteristics of Dilute Water Based Al₂O₃–Cu Hybrid Nanofluids. *Journal of Nanoscience and Nanotechnology* **2014**, *14*, 2563-2572, <https://doi.org/10.1166/jnn.2014.8467>.
26. Gul, T.; Bilal, M.; Shuaib, M.; Mukhtar, S.; Thounthong, P. Thin film flow of the water-based carbon nanotubes hybrid nanofluid under the magnetic effects. *Heat Transfer* **2020**, *49*, 3211-3227, <https://doi.org/10.1002/htj.21770>.
27. Li, Z.; Shahsavari, A.; Niazi, K.; Al-Rashed, A.A.A.A.; Rostami, S. Numerical assessment on the hydrothermal behavior and irreversibility of MgO-Ag/water hybrid nanofluid flow through a sinusoidal hairpin heat-exchanger. *International Communications in Heat and Mass Transfer* **2020**, *115*, <https://doi.org/10.1016/j.icheatmasstransfer.2020.104628>.
28. Dogonchi, A. S.; Waqas, M.; Seyyedi, S. M.; Hashemi-Tilehnoee, M.; Ganji, D. D. Numerical simulation for thermal radiation and porous medium characteristics in flow of CuO-H₂O nanofluid. *Journal of the Brazilian Society of Mechanical Sciences and Engineering* **2019**, *41*, 1-13, <https://doi.org/10.1007/s40430-019-1752-5>.
29. Sravan Kumara, T.; Dinesh, P. A.; Makinde, O.D. Impact of Lorentz Force and Viscous Dissipation on Unsteady Nanofluid Convection Flow over an Exponentially Moving Vertical Plate. *Mathematical Models and Computer Simulations*, **2020**, *12*, 631-646, <https://doi.org/10.1134/s2070048220040110>.